NANO LETTERS

pubs.acs.org/NanoLett

Fano Resonances in Plasmonic Nanoclusters: Geometrical and Chemical Tunability

J. Britt Lassiter,[†,‡] Heidar Sobhani,[‡,§] Jonathan A. Fan,[⊥] Janardan Kundu,[‡,∥] Federico Capasso,[⊥] Peter Nordlander*[,†,‡,§] and Naomi J. Halas*[,†,‡,§,∥]

[†]Department of Physics and Astronomy, [‡]Laboratory for Nanophotonics, [§]Department of Electrical and Computer Engineering, and [∥]Department of Chemistry, Rice University, Houston, Texas 77005 and [⊥]School of Engineering and Applied Sciences, Harvard University, 29 Oxford Street, Cambridge, Massachusetts 02138

ABSTRACT Clusters of plasmonic nanoparticles and nanostructures support Fano resonances. Here we show that this spectral feature, produced by the interference between bright and dark modes of the nanoparticle cluster, is strongly dependent upon both geometry and local dielectric environment. This permits a highly sensitive tunability of the Fano dip in both wavelength and amplitude by varying cluster dimensions, geometry, and relative size of the individual nanocluster components. Plasmonic nanoclusters show an unprecedented sensitivity to dielectric environment with a local surface plasmon resonance figure of merit of 5.7, the highest yet reported for localized surface plasmon resonance sensing in a finite nanostructure.

KEYWORDS Plasmon, Fano resonance, nanocluster, coherent phenomena, localized surface plasmon resonance (LSPR), sensing, figure of merit (FoM)

The coupling between metallic nanoparticles in aggregates supports collective electronic oscillations, known as surface plasmons, of the entire structure; this is a topic of intense current interest.[1] Each type of nanoparticle cluster, such as a nanoparticle dimer,[2−4] trimer,[5−7] quadrumer,[8,9] tetramer,[10] and so forth,[11−15] exhibits its own unique set of collective plasmon modes arising from the interaction between the plasmons supported by each nanoparticle in the cluster. These collective plasmon modes can be excited at distinct energies that depend on the relative phase of the plasmon oscillations in the individual nanoparticles of the complex. Since surface plasmons are well described as classical oscillators with resonances at optical frequencies, interacting nanoparticles are in essence systems of coupled oscillators, supporting a rich array of phenomena, such as electromagnetically induced transparency (EIT) and Fano resonances (FRs).[16−23] Geometries ranging from mismatched nanoparticle pairs,[3] "dolmen" structures,[24] coupled ring-disk systems,[25−27] heptamers,[1,28−30] and layered nanoparticles[31] have all been shown to support EIT and FRs. Because the coherent coupled oscillator response is essentially an interference phenomenon dependent upon the relative phase of the constituent oscillators, it is highly sensitive to perturbations such as symmetry breaking, local variations in geometry, and dielectric environment.[25,29,32] This inherent sensitivity has spurred interest in coupled structures, which promise to provide a higher sensitivity optical response than uncoupled plasmonic systems.

Here we examine how the coherent properties of a nanoscale plasmonic cluster are affected by cluster size, geometry, and local dielectric environment. Our study focuses primarily on the seven-member "heptamer" cluster. We examine the important case of how local changes in dielectric environment modify the frequency of the FR of the cluster. Heptamers have been predicted to have extremely large spectral shifts of their FR induced by changes in the surrounding refractive index.[29] In this paper we show that, as predicted, the FR in heptamers exhibits an unusually large shift with changes in refractive index; in fact, this structure exhibits the largest localized surface plasmon resonance (LSPR) response of any known nanostructure, assessed in terms of the figure of merit (FoM) of the cluster aggregate.[33,34]

The plasmonic structures investigated in this letter were fabricated by electron beam lithography and are composed of 30 nm thick Au disks on a 1 nm Ti adhesion layer, evaporated onto a Si substrate coated with a 100 nm thick silicon dioxide layer. The dielectric permittivity of the substrate is therefore similar to a typical glass substrate.

In Figure 1, we show the scattering spectra of three heptamers of increasing size. As can be seen from the SEM images of the clusters in the top panels, the dimensions of the particle radii are increased while the gap sizes are kept constant at ∼15 nm (Figure 1A−C (i)). The scattering spectrum of each cluster was collected using dark-field microspectroscopy (Figure 1A−C (ii)). (The microscope used was a Zeiss Axiovert 200 MAT, the CCD was a Princeton Instruments Pixis 400 BR, and the spectrograph was an Acton 2156i imaging spectrograph.) The specific microscope

* To whom correspondence should be addressed. E-mail: (N.J.H.) halas@rice.edu; (P.N.) nordland@rice.edu.

Received for review: 06/15/2010
Published on Web: 07/16/2010

DOI: 10.1021/nl102108u | *Nano Lett.* **2010,** *10,* 3184–3189

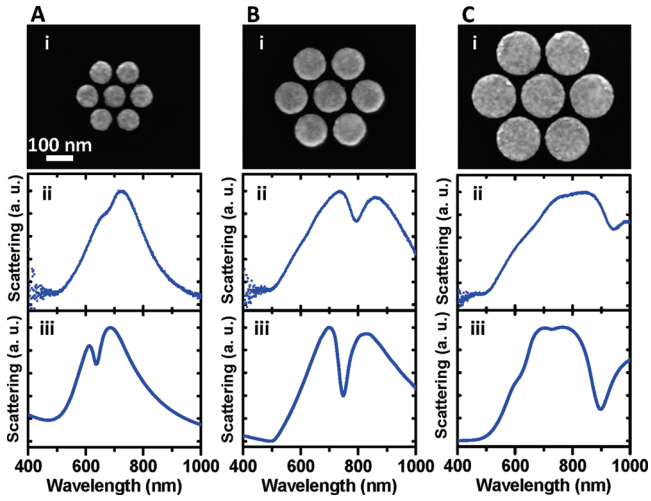

FIGURE 1. Size dependence of the scattering spectrum of a heptamer: (A) 85 nm diameter constituent particles; (B) 128 nm diameter particles; (C) 170 nm diameter particles. In all cases, the gap sizes between the particles in the heptamers were nominally ~15 nm. (i) SEM images obtained using an FEI Quanta 400 SEM; (ii) experimentally obtained dark-field scattering spectra, obtained with unpolarized light, of each individual cluster shown in (i); (iii) FDTD calculations of the dark-field spectral response of the same structure.

objective used was critical to our ability to observe the FR. For all of the data reported here, the objective characteristics were angle of incidence = ~50° from the surface normal, numerical aperture (NA) = 0.4. The FRs were not as pronounced when using objectives with higher incidence angles or numerical apertures. Because these structures are not in the quasistatic limit, retardation effects are present when light is incident from large angles with respect to the substrate normal. In this case, the retardation effects allow direct excitation of the subradiant mode,[25] effectively limiting the interference effect that causes the Fano resonance. This Fano interference effect is described below in detail.

Theoretical scattering spectra for these structures were obtained using the finite-difference time-domain (FDTD) method (Figure 1A–C (iii)). The dielectric function used to model Au was obtained from the experimental data of Johnson and Christy (JC).[35] The clusters were simulated on an infinite dielectric substrate with $\varepsilon = 2.04$ to represent the experimental supporting substrate and illuminated with oblique incident light. The back scattered light in the simulation was recorded over a conical solid angle corresponding to the numerical aperture of the objective lens used in the experiment.

The optical properties of symmetric plasmonic heptamers composed of spherical and cylindrical nanoparticles have been analyzed and described in several recent publications.[1,28–30] The symmetry group of the heptamer is D_{6h}. Using the plasmon hybridization concept, the plasmon modes can be classified according to their irreducible representations. The collective modes that can couple efficiently to light are the E_{1u} modes. The two relevant modes for Fano interference are (1) a bonding bright (superradiant) mode where the dipolar plasmons of all nanoparticles oscillate in phase and in the same direction, and (2) an antibonding dark (subradiant) mode, where the dipolar moment of the center particle opposes the dipole moment of the surrounding ring. In the quasistatic, nonretarded limit, the dark mode possesses nearly no net dipole moment and does not easily couple to light. In the retarded limit, the bright mode becomes superradiant, while the dark mode remains subradiant. Also in this limit, the weak coupling mediated by the plasmonic near-field introduces an interaction between the sub- and superradiant modes, inducing a FR in the superradiant continuum at the energy of the subradiant mode. Because of its D_{6h} symmetry, the optical properties of the cluster, including its FR, are isotropic, that is, independent of the orientation of the in-plane polarization of light incident on the structure.

Figure 1 shows the evolution of the scattering spectrum of a heptamer as the cluster is scaled up from the near-quasistatic to the fully retarded limit. The Fano minimum is strongly dispersive toward lower energies with increasing cluster size, and the Fano line shape becomes broadened. The smallest heptamer (A) exhibits a relatively narrow plasmon resonance near 700 nm, which is the bright superradiant bonding E_{1u} mode. Since the overall structure size is small, this mode does not radiate strongly and is quite narrow. A very weak FR appears in the theoretical spectrum and appears only as a weak modulation (at nominally 690 nm) in the experimental spectrum of the cluster. For the intermediate size heptamer in (B), the bright mode is red shifted to approximately 750 nm and significantly broadened due to the increased radiation damping. The FR at 750 nm is now very pronounced. For the largest heptamer (C), the superradiant mode shifts to nominally 900 nm and is dramatically broadened. A strong FR is induced at 900 nm. For a heptamer this large, the subradiant mode radiates slightly, resulting in a slight broadening of the line width of the FR. Interestingly, the subradiant mode appears to redshift slightly more strongly than the superradiant mode with increasing size of the heptamers. This effect likely occurs because the antibonding subradiant mode contains a significant admixture of higher order modes, while the superradiant is mostly dipolar in nature. Since the gap size is kept constant, larger diameter disks result in stronger plasmonic interactions between the individual disks and consequently stronger hybridization. Because of this stronger hybridization of the higher order modes, the subradiant mode redshifts more than the superradiant mode for increasing heptamer size in the present size range.

In Figure 2, an example of the effect of symmetry breaking on the optical spectrum of the heptamer is shown. One of the peripheral particles of a heptamer is removed, resulting in an incomplete ring of nanostructures surrounding the center particle. The optical response of this reduced symmetry structure is no longer isotropic. To study the

DOI: 10.1021/nl102108u | *Nano Lett.* **2010,** *10,* 3184–3189

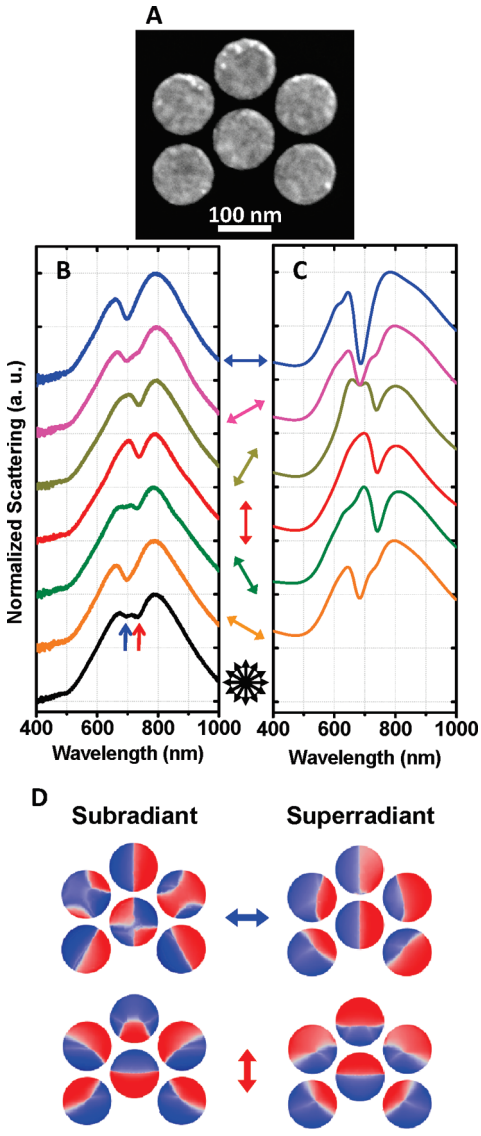

FIGURE 2. Asymmetric heptamers. (A) SEM image of heptamer. The disk diameters are 128 nm with ~15 nm gaps. (B) Experimental dark-field scattering spectra of the asymmetric heptamer, obtained with unpolarized incident and polarization-analyzed scattered light. Colored arrows show the polarization angle with respect to the particle, as in the SEM image. Polarized spectra were collected at 30° angular increments. The black curve is unpolarized data. (C) FDTD simulations corresponding to the experimental spectra in (B). (D) Charge plots calculated using FEM for the subradiant (left) and superradiant (right) modes for the two fundamental polarizations of the structure depicted by the arrows.

polarization dependence of the spectral response of this cluster, a rotating analyzer (Zeiss) is inserted in the collection optics of the microscope. Thus, the nanoparticle is still excited using unpolarized light, but the scattered light is polarized just before collection. In Figure 2B,C, we show the measured and calculated scattering spectra for different polarization collection angles. As for the case of the isotropic, complete heptamer, the spectrum is characterized by a broad superradiant mode centered around 700 nm. However, with reduced symmetry the Fano interference displays a more complex behavior. For horizontal polarization (blue), a clear FR appears at 700 nm, and for vertical polarization (red), it appears at 740 nm. For other polarizations, the scattering spectra exhibit a mixture of these two resonances.

A calculation of the induced charge densities of this reduced-symmetry cluster reveals the microscopic origin of the unusual split-FR observable in this structure (Figure 2D). These calculations were performed using a commercial (COMSOL) implementation of the Finite Element Method (FEM). For both polarizations, the subradiant charge plots were calculated at the wavelength of the Fano minimum (Figure 2D, left) and the superradiant charge plots were obtained for the maximum at the long-wavelength side of the Fano dip (Figure 2D, right). The superradiant charge plots clearly show that the dipolar components of all constituent particles are oriented in the same direction, resulting in the enhanced radiative damping and resultant broadening characteristic of superradiant modes. For the subradiant modes, however, the charge plots are distinctly different. For horizontal polarization, the subradiant mode has a strong admixture of nanoparticle quadrupoles. This hybridization is caused by the absence of a symmetry axis along the polarization vector. For vertical polarization, the subradiant mode is mostly a dipolar mode with the in-phase dipolar contribution of the two center particles opposing the dipole moment of the surrounding four particles, similar to the case of the fully symmetric heptamer.

Fano resonances can be realized in other symmetric clusters consisting of a center particle surrounded by a ring of particles. The reason for the very pronounced FR in the heptamer (Figure 1) is the almost perfect cancellation of the total dipole moment of the ring of particles and the (out-of-phase) center particle in the subradiant mode. For a larger ring, such as the homo-octamer shown in Figure 3A (i), the dipole moment of the ring will become larger than that of the center particle. For such a structure, the antibonding mode will have a finite dipole moment and couple efficiently to incident light. The conditions for a FR are thus not satisfied. Neither the experimental nor the calculated spectra in Figure 3A show a pronounced FR. However, by making the diameter of the center particle larger, its dipole moment increases. For a sufficiently large center particle, its dipole moment can become equal to that of the surrounding ring. For such a hetero-octamer consisting of particles of different sizes, the antibonding mode becomes subradiant, and a strong FR with a very deep minimum, approaching transparency, is induced around 800 nm as shown in Figure 3B.

Much of the current interest in FR in plasmonic system stems from their potential as efficient LSPR sensors.[32,33,36−38] The complex interference phenomena underlying the formation of FRs in coupled plasmonic systems are highly sensitive to the dielectric environment in the junctions of the overall structure. In addition, FRs are typically very narrow, which allows for a more precise measurement of small peak shifts induced by changes in the dielectric properties of the

DOI: 10.1021/nl102108u | *Nano Lett.* **2010,** *10,* 3184–3189

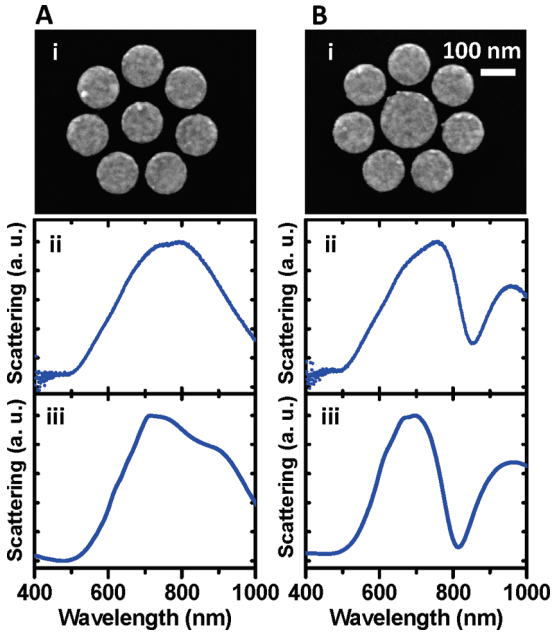

FIGURE 3. Scattering spectra of octamers. (A) Homo-octamer SEM image (i), dark-field scattering spectrum (ii) and FDTD simulation (iii). All particles have the same diameter =128 nm. This results in a gap of ~15 nm between the outer particles and a gap of ~40 nm between the inner particle and outer ring. (B) Hetero-octamer SEM image (i), dark-field scattering spectrum (ii), and FDTD simulation (iii). Here, the inner particle was enlarged such that all gaps were the same size (~15 nm). This resulted in an inner particle diameter =175 nm and the outer particle diameter =128 nm. All fabrication and data collection procedures are the same here as for Figure 1. All data were obtained with unpolarized light.

nanostructure environment. The LSPR efficiency of a plasmonic nanoparticle is typically evaluated by its FoM, defined as the ratio of the plasmon energy shift per refractive index unit change in the surrounding medium, divided by the width of the spectral peak.[33] For asymmetric FRs, we define the energy of the resonance as the midpoint between the energy of first maximum and the energy of the minimum. The width is defined as the energy difference between those spectral features. This definition for the spectral width used to calculate the FoM has been suggested before[25] and is required because the asymmetric line shape associated with Fano resonances leads to an ill-defined full width at half-maximum (fwhm), as is usually used in the case of ordinary, or peaklike, plasmon resonances.[33] Theoretical predictions for FoM for individual plasmonic nanostructures range from 7 for coupled dipole−quadrupole antennas,[32] 8 for noncentric planar ring-disk cavities,[25] to 11 for a symmetric silver sphere heptamer.[29] The recent experimental demonstration of a FoM of 3.8 for a coupled dipole−quadrupole antennas[32] show the tremendous potential for FR-based LSPR sensing.

To investigate the LSPR sensitivity of the planar heptamer, we performed dark-field scattering spectroscopy on individual heptamers embedded in various dielectric media: methanol (n = 1.326),[39] butanol (n = 1.397),[39] index matching oil (n = 1.506, Cargille Laboratories

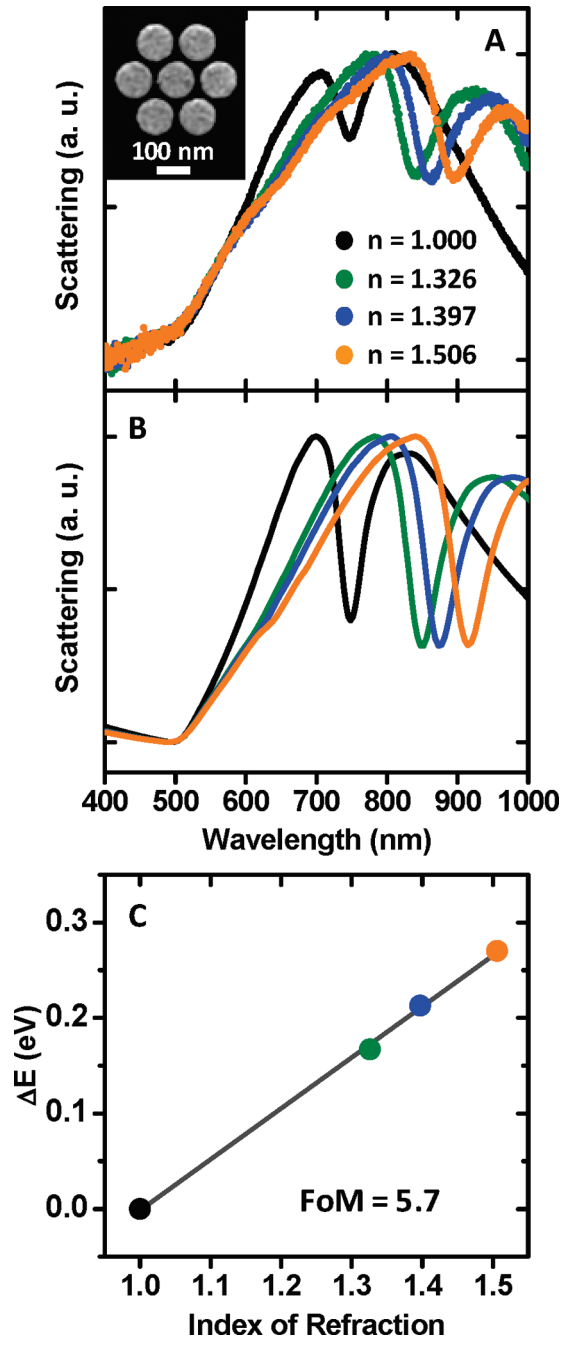

FIGURE 4. LSPR sensing in heptamers. (A) LSPR sensing for heptamer of same dimensions as reported in Figure 1. Four polarized scattering spectra are shown for different media (air, black), (methanol, green), (butanol, blue), (immersion oil, orange). The values for the refractive indices of each medium are shown in the figure. (B) FDTD simulations corresponding to the experiment. (C) Linear plot of the LSPR shifts of the FR vs refractive index of the embedding medium.

internal documentation). For each medium, the entire substrate was first rinsed in that medium and then fully immersed in the medium in a glass-bottom Petri dish (Ted Pella). The scattering spectra were obtained from the immersed samples. Figure 4 shows a very pronounced redshift of the FR with increasing refractive index of the surrounding medium. In air ambient, the FR appears at

DOI: 10.1021/nl102108u | Nano Lett. 2010, 10, 3184–3189

750 nm, and in immersion oil with a refractive index $n = 1.5$, the FR is shifted to 900 nm. To quantify the LSPR sensitivity, we obtain the slope of the best-fit line (linear regression with a slope =0.53) for the energy of the FR as a function of surrounding dielectric permittivity, and divide by the Fano line width (0.093 eV). The resulting FoM is 5.7, which to our knowledge is the highest LSPR FoM reported so far for an individual finite nanostructure. The FoM calculated from the theoretical simulations (Figure 4B) is slightly smaller (5.1). From this we can infer that the nanostructures were likely completely coated by each solvent medium, if this was not the case, the theoretical FoM would be larger than that obtained experimentally.

While this current result indicates great promise for significantly increasing LSPR sensitivities by focusing on FRs, the full potential for FR-based LSPR sensing is clearly not yet realized. In none of the structures studied in these initial experiments has the LSPR FoM been optimized. By using larger structures or structures with narrower gaps, it is highly likely that an even larger FoM can be achieved. Structures fabricated in silver instead of gold, should also yield even larger FoM than those reported here, since the lattice polarizability and electromagnetic screening of silver is significantly smaller than for gold. An advantage with lithographically fabricated clusters such as the present structure is that the energies of the FRs can be tuned very accurately by varying the ratio of the disk thickness to cluster diameter.

In conclusion, we have shown that lithographically fabricated nanoscale plasmonic clusters exhibit pronounced FRs, which depend strongly on both the geometry and the dielectric environment of the complex. By changing the size of a heptamer, it is possible to tune the FR to different wavelengths. By symmetry breaking, one can further tune the wavelength of the FR and induce new resonances. A very deep FR, approaching transparency can be induced in an octamer cluster consisting of a center particle surrounded by a ring of seven particles if the size of the center particle is sufficiently large. We have also shown experimentally that FRs of heptamer clusters possess exceptional LSPR sensitivities. For a heptamer consisting of seven particles of the same size, we measure a FoM of 5.7. This unparalleled LSPR sensitivity, found in a cluster fabricated by readily available nanofabrication methods, is likely to stimulate increased interest and applications in sensing and detection based on coherent plasmonic phenomena.

Acknowledgment. This work was supported by Robert A. Welch Foundation under Grants C-1220 (N.J.H) and C-1222 (P.N.), and Department of Defense National Security Science and Engineering Faculty Fellowship (N.J.H) via Grant N00244-09-0067 and the Center for Advanced Solar Photophysics, an Energy Frontier Reseach Center funded by the U.S. Department of Energy (P.N. and N.J.H.). J.F. and F.C. acknowledge funding by the NSF NIRT under Grant 0709323. Computations were supported in part by the Shared University Grid at Rice funded by NSF under Grant EIA-0216467 and a partnership between Rice University, Sun Microsystems, and Sigma Solutions, Inc. We also thank Dr. Nikolay A. Mirin, Mark W. Knight, and Jared Day for helpful discussions.

Supporting Information Available. An additional figure is presented. This material is available free of charge via the Internet at http://pubs.acs.org.

REFERENCES AND NOTES

(1) Fan, J. A.; Wu, C. H.; Bao, K.; Bao, J. M.; Bardhan, R.; Halas, N. J.; Manoharan, V. N.; Nordlander, P.; Shvets, G.; Capasso, F. *Science* **2010**, *328* (5982), 1135–1138.
(2) Rycenga, M.; Camargo, P. H. C.; Li, W.; Moran, C. H.; Xia, Y. N. *J. Phys. Chem. Lett.* **2010**, *1*, 696–703.
(3) Brown, L. V.; Sobhani, H.; Lassiter, J. B.; Nordlander, P.; Halas, N. J. *ACS Nano* **2010**, *4*, 819–832.
(4) Pakizeh, T.; Kall, M. *Nano Lett.* **2009**, *9*, 2343–2349.
(5) Mastroianni, A. J.; Claridge, S. A.; Alivisatos, A. P. *J. Am. Chem. Soc.* **2009**, *131* (24), 8455–8459.
(6) Li, Z. P.; Shegai, T.; Haran, G.; Xu, H. X. *ACS Nano* **2009**, *3* (3), 637–642.
(7) Shegai, T.; Li, Z. P.; Dadosh, T.; Zhang, Z. Y.; Xu, H. X. *Proc. Natl. Acad. Sci. U.S.A.* **2008**, *105*, 16448–16453.
(8) Brandl, D. W.; Mirin, N. A.; Nordlander, P. *J. Phys. Chem. B* **2006**, *110* (25), 12302–12310.
(9) Zhang, Z.; Weber-Bargioni, A.; Wu, S. W.; Dhuey, S.; Cabrini, S.; Schuck, P. J. *Nano Lett.* **2009**, *9* (12), 4505–4509.
(10) Urzhumov, Y. A.; Shvets, G.; Fan, J.; Capasso, F.; Brandl, D.; Nordlander, P. *Opt. Express* **2007**, *15* (21), 14129–14145.
(11) Chen, H. J.; Sun, Z. H.; Ni, W. H.; Woo, K. C.; Lin, H. Q.; Sun, L. D.; Yan, C. H.; Wang, J. F. *Small* **2009**, *5* (18), 2111–2119.
(12) Gomez, D. E.; Vernon, K. C.; Davis, T. J. *Phys. Rev. B.* **2010**, *81*, No. 075414.
(13) Liu, H.; Liu, Y. M.; Li, T.; Wang, S. M.; Zhu, S. N.; Zhang, X. *Phys. Status Solidi B* **2009**, *246* (7), 1397–1406.
(14) Hossain, M. K.; Huang, G. G.; Kaneko, T.; Ozaki, Y. *Chem. Phys. Lett.* **2009**, *477* (1−3), 130–134.
(15) Jin, R. *Angew. Chem., Int. Ed.* **2010**, *49*, 2826–2829.
(16) Liu, N.; Kaiser, S.; Giessen, H. *Adv. Mater.* **2008**, *20* (23), 4521–4525.
(17) Liu, N.; Liu, H.; Zhu, S. N.; Giessen, H. *Nat. Photonics* **2009**, *3* (3), 157–162.
(18) Chen, Y. T.; Chern, R. L.; Lin, H. Y. *Appl. Opt.* **2010**, *49* (15), 2819–2826.
(19) Burrows, C. P.; Barnes, W. L. *Opt. Express* **2010**, *18* (3), 3187–3198.
(20) Yang, Z. J.; Zhang, Z. S.; Zhang, W.; Hao, Z. H.; Wang, Q. Q. *Appl. Phys. Lett.* **2010**, *96*, 13113.
(21) Fedotov, V. A.; Papasimakis, N.; Plum, E.; Bitzer, A.; Walther, M.; Kuo, P.; Tsai, D. P.; Zheludev, N. I. *Phys. Rev. Lett.* **2010**, *104*, 223901.
(22) Su, X. R.; Zhang, Z. S.; Zhang, L. H.; Li, Q. Q.; Chen, C. C.; Yang, Z. J.; Wang, Q. Q. *Appl. Phys. Lett.* **2010**, *96* (4), 743113.
(23) Pakizeh, T.; Langhammer, C.; Zoric, I.; Apell, P.; Kall, M. *Nano Lett.* **2009**, *9*, 882–886.
(24) Verellen, N.; Sonnefraud, Y.; Sobhani, H.; Hao, F.; Moshchalkov, V. V.; Dorpe, P. V.; Nordlander, P.; Maier, S. A. *Nano Lett.* **2009**, *9* (4), 1663–1667.
(25) Hao, F.; Sonnefraud, Y.; Dorpe, P. V.; Maier, S. A.; Halas, N. J.; Nordlander, P. *Nano Lett.* **2008**, *8* (11), 3983–3988.
(26) Hao, F.; Nordlander, P.; Sonnefraud, Y.; Dorpe, P. V.; Maier, S. A. *ACS Nano* **2009**, *3* (3), 643–652.
(27) Sonnefraud, Y.; Verellen, N.; Sobhani, H.; Vandenbosch, G. A. E.; Moshchalkov, V. V.; Van Dorpe, P.; Nordlander, P.; Maier, S. A. *ACS Nano* **2010**, *4* (3), 1664–1670.

DOI: 10.1021/nl102108u | *Nano Lett.* **2010,** *10,* 3184–3189

(28) Le, F.; Brandl, D. W.; Urzhumov, Y. A.; Wang, H.; Kundu, J.; Halas, N. J.; Aizpurua, J.; Nordlander, P. *ACS Nano* **2008**, *2* (4), 707–718.
(29) Mirin, N. A.; Bao, K.; Nordlander, P. *J. Phys. Chem. A* **2009**, *113* (16), 4028–4034.
(30) Hentschel, M.; Saliba, M.; Vogelgesang, R.; Giessen, H.; Alivisatos, A. P.; Liu, N. Nano Lett. [Online early access]. DOI:10.1021/nl101938p.
(31) Mukherjee, S.; Sobhani, H.; Lassiter, J. B.; Bardhan, R.; Nordlander, P.; Halas, N. J. Nano Letters [Online early access]. DOI: 10.1021/nl1016392.
(32) Liu, N.; Weiss, T.; Mesch, M.; Langguth, L.; Eigenthaler, U.; Hirscher, M.; Sonnichsen, C.; Giessen, H. *Nano Lett.* **2010**, *10* (4), 1103–1107.
(33) Sherry, L. J.; Chang, S. H.; Schatz, G. C.; Van Duyne, R. P.; Wiley, B. J.; Xia, Y. N. *Nano Lett.* **2005**, *5* (10), 2034–2038.
(34) Liao, H. W.; Nehl, C. L.; Hafner, J. H. *Nanomedicine* **2006**, *1*, 201–206.
(35) Johnson, P. B.; Christy, R. W. *Phys. Rev. B* **1972**, *6*, 4370–4379.
(36) Jonsson, M. P.; Dahlin, A. B.; Jonsson, P.; Hook, F. *Biointerphases* **2008**, *3* (3), FD30–FD40.
(37) Vo-Dinh, T.; Dhawan, A.; Norton, S. J.; Khoury, C. G.; Wang, H. N.; Misra, V.; Gerhold, M. D. *J. Phys. Chem. C* **2010**, *114* (16), 7480–7488.
(38) Mayer, K. N.; Hao, F.; Lee, S. H.; Nordlander, P.; Hafner, J. H. *Nanotechnology* **2010**, *21*, 255503.
(39) El-Kashef, H. *Physica B* **2000**, *279*, 295–301.

DOI: 10.1021/nl102108u | *Nano Lett.* **2010,** *10,* 3184–-3189